Signature of Dirac semimetal states in gray arsenic studied by de Haas–van Alphen and Shubnikov–de Haas quantum oscillations

Linlin An,[1,2] Xiangde Zhu,[1] Yuting Qian,[3,4] Chuanying Xi,[1] Wei Ning,[1,*] Hongming Weng,[3,4,5,6] and Mingliang Tian[1,7,8,†]

[1]*Anhui Province Key Laboratory of Condensed Matter Physics at Extreme Conditions, High Magnetic Field Laboratory, Chinese Academy of Sciences, Hefei 230031, Anhui, China*

[2]*Department of Physics, University of Science and Technology of China, Hefei 230026, China*

[3]*Beijing National Laboratory for Condensed Matter Physics, and Institute of Physics, Chinese Academy of Sciences, Beijing 100190, China*

[4]*University of Chinese Academy of Sciences, Beijing 100049, China*

[5]*Songshan Lake Materials Laboratory, Dongguan, Guangdong 523808, China*

[6]*CAS Center for Excellence in Topological Quantum Computation, University of Chinese Academy of Sciences, Beijing 100190, China*

[7]*School of Physics and Materials Sciences, Anhui University, Heifei 230601, China*

[8]*Collaborative Innovation Center of Advanced Microstructures, Nanjing University, Nanjing 210093, China*

(Received 8 September 2019; revised manuscript received 4 February 2020; accepted 6 April 2020; published 7 May 2020; corrected 2 July 2020)

We report systematically studies of de Haas–van Alphen (dHvA) and Shubnikov–de Haas (SdH) quantum oscillations under high magnetic fields on gray arsenic, which has been suggested to be a topological insulator by first-principles calculations and angle-resolved photoemission spectroscopy. We observed large unsaturated magnetoresistance and pronounced quantum oscillations in two methods. By analysis of these quantum oscillation spectra, we obtained two major frequency branches around 3.8–18 and 153–162 T, and the light effective quasiparticle mass and nontrivial Berry phase. These results suggest that bulk crystals of gray arsenic may belong to the category of topological Dirac semimetals rather than topological insulators.

DOI: 10.1103/PhysRevB.101.205109

I. INTRODUCTION

Topological materials, in which the topology of electronic bands in bulk materials lead to robust, unconventional surface states and electromagnetic activity, have attracted much attention because of their potential applications in hydrogen evolution catalysis [1,2], plasmonics [3–6], and next-generation electronic devices [7–10]. While recent theoretical work [11–13] has predicted a few thousand potential candidates with a topological nature based on various symmetry indicators, only a small number of realistic materials were experimentally confirmed to be topological, including time-reversal [14,15], mirror-symmetric and nonsymmorphic topological insulators [16,17], Dirac [18,19], Weyl [20–22], nodal-chain semimetals [23], new fermions [24], and so on. Except for the difficulty in synthesizing these predicted materials, there are still very few efficient ways to identify the topological character of a material. One of the most popular and direct techniques is angular-resolved photoemission spectroscopy (ARPES) [25], where the band structures with linearly dispersed crossing near the Fermi surface can be recognized, but this technique is limited by the sample surface quality and the zero-magnetic-field condition. Another important way is to detect the electromagnetic responses combining electrical transport and magnetization measurements, such as by measuring the negative magnetoresistance due to the chiral anomaly [26], the oscillations of magnetoresistance (MR), or magnetization, i.e., the Shubnikov–de Haas (SdH) [27,28] or the de Haas–van Alphen (dHvA) effect [29] under high magnetic fields due to the Landau level quantization, where the topological-related Berry phase as well as the band structures can be identified.

Gray arsenic, which is a black phosphorene analog, has recently attracted attention in the search for two-dimensional (2D) materials with high mobility and excellent contact with electronic materials [30]. ARPES experiments and first-principles calculations have revealed a topological insulator state [31], but recently SdH oscillation studies of gray arsenic single crystals indicated that this state has a strong signature of Dirac fermion characters [32]. Here we exhibited systematically both the dHvA and SdH effect measurements on gray arsenic single crystals. The analysis of quantum oscillations demonstrated that this material harbors nearly massless relativistic fermions along with a nontrivial Berry phase. From fast Fourier transform spectra, two major frequency branches were identified near 18 and 162 T by the SdH effect, or 3.8 and 153 T by the dHvA effect, indicating that there exists at least two pockets near the Fermi surface. We found that both experiments gave almost the same frequency value near 160 T, but the lower one shows a significant difference between the two techniques, which was not discovered in a previous SdH

*Author to whom all correspondence should be addressed: ningwei@hmfl.ac.cn

†tianml@hmfl.ac.cn

 ©2020 American Physical Society

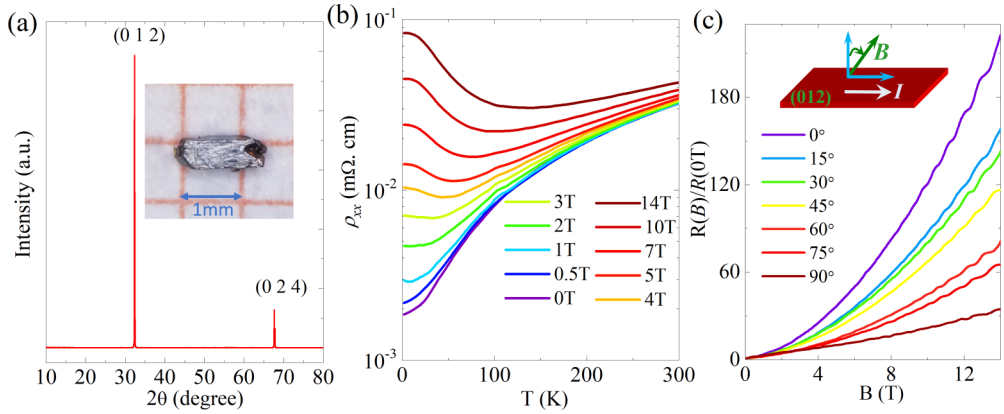

FIG. 1. (a) X-ray diffraction pattern of gray arsenic single crystal. The inset shows an optical image of a typical crystal. (b) Temperature dependence of resistivity at a different magnetic field perpendicular to the (012) surface plane. (c) Angular dependence of magnetoresistance (MR), $R_{xx}(B)/R_{xx}(0T)$, at 2 K.

study [24]. Analysis of the data provides evidence of the nontrivial Berry phase for both bands, indicating that gray arsenic may be a Dirac semimetal.

II. EXPERIMENTAL METHOD

Gray arsenic single crystals were synthesized by the Bi flux method. The obtained crystals show an elongated rectangular shape, as shown in the inset of Fig. 1(a). Phase purity and structural analysis of the single crystals was done using the high-resolution powder x-ray diffraction (XRD) technique with Cu $K\alpha$ radiation. Magnetization was measured using a superconducting quantum interference device magnetometer (SQUID, Quantum Design, Inc.). Figure 1(a) shows the XRD patterns of a crystal. The sharp reflection peaks indicate that the crystals have high crystallinity with a (012) surface plane, which is different from that reported previously with a (001) surface plane. Electrical transport measurements were performed with the four-probe technique on the rectangular crystal with a 14 T physical properties measurement system (PPMS, Quantum Design) and the 40 T hybrid magnet in the High Magnetic Field Laboratory in Hefei, China.

The band structure is calculated by the Vienna ab initio simulation package (VASP) [33] with the projector augmented wave method [34,35]. The exchange-correlation potential is the Perdew-Burke-Ernzerhof (PBE) type generalized gradient approximation (GGA) of Ref. [36]. The crystal structure parameters employed in our calculations were from the Inorganic Crystal Structure Database (ICSD). The k-mesh in the self-consistent process for the Brillouin zone (BZ) integration was set as $10 \times 10 \times 10$. The electronic structures without and with spin-orbit coupling (SOC) were carried out. The Fermi surface (FS) was calculated using the interpolation technique with WANNIER90 [37] and WANNIERTOOLS [38] packages based on maximally localized Wannier functions. The Wannier functions have been generated for As p orbitals.

III. RESULTS AND DISCUSSION

Figure 1(b) shows the magnetotransport properties of gray arsenic with the magnetic field perpendicular to the (012) surface plane and the current direction. The temperature dependence of resistivity at zero magnetic field displays metallic behavior with decreasing temperature down to 2 K. With application of a magnetic field, an upturn of resistivity in the low-temperature range was found. This magnetic-field-induced enhancement of resistivity was also observed in many other semimetals, such as TaP, NbP, WTe_2, and TaAs [39–42].

Figure 1(c) shows the angle-dependent MR, $R_{xx}(B)/R_{xx}(0\,\mathrm{T})$, by tilting magnetic fields from $\theta = 0^\circ$ to parallel to the electric current ($\theta = 90^\circ$) at 2 K, where the θ is defined as the angle between the magnetic field and the vector normal to the surface plane. The MR shows a semiclassical quadratic field dependence in the low-field range, while it becomes quasilinear and is accompanied by significant resistance oscillations in the high-field range. As the applied magnetic field is tilted from $\theta = 90^\circ$ to 0°, the MR increases about 560% at 14 T. Such a large variation indicates an anisotropy of the electronic structure because the orbit effect of the MR caused by the change of the current orientation with respect to the magnetic field is usually less than 10% for a regular metal. By analyzing the corresponding oscillation spectra, these resistance oscillations are from the Landau quantization of the energy levels, i.e., the well-known Shubnikov–de Haas (SdH) oscillations.

As shown in Fig. 1, the MR shows no saturation with magnetic fields up to 14 T. To further investigate the MR behavior, we performed MR measurements at $\theta = 0^\circ$ with magnetic fields up to 40 T by using the hybrid-magnet in the High Magnetic Field Laboratory in Hefei, China. Figure 2(a) presents the resistance versus magnetic fields at different temperatures. After subtracting a smooth background from the R_{xx} [see Fig. 2(a)], we obtained the oscillatory component of resistance versus $1/B$ at various temperatures, as shown in Fig. 2(b). Compared with the low-field MR data shown in Fig. 1(c), a clear Landau level splitting is observed in the high-magnetic-field range, as shown in the inset of Fig. 2(b). The splitting can be ascribed to Zeeman splitting, which is gradually smeared out with the increase of temperature above 30 K. The fast Fourier transfer (FFT) of ΔR_{xx} [Fig. 2(b)] yields two major frequencies of $F_\beta = 18$ T and $F_\gamma = 162$ T with their harmonic frequencies $F_{2\gamma} = 324$ T, $F_{3\gamma} = 486$ T, and $F_{4\beta+\gamma} = 234$ T. The lower frequency $F_\beta = 18$ T was not recognized in a previous report [24], probably due to

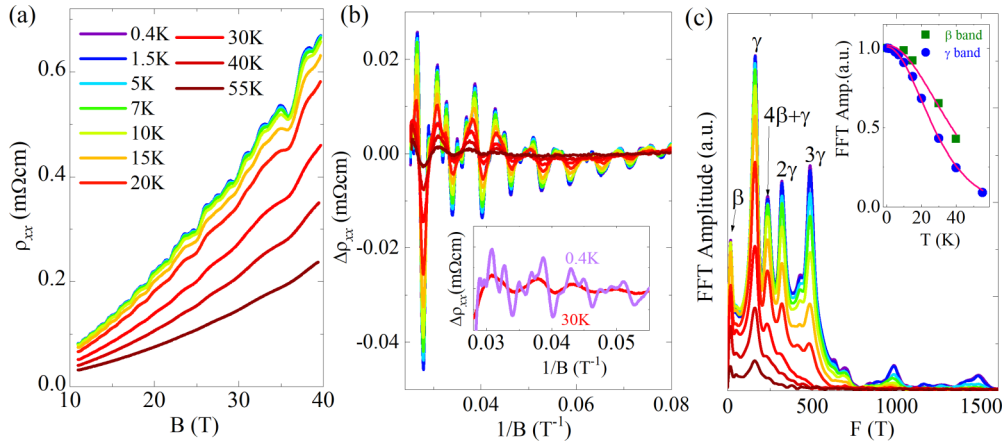

FIG. 2. (a) Magnetic field dependence of resistance at various temperatures under magnetic fields up to 40 T, with the field perpendicular to the (012) plane. (b) The oscillatory components of resistance at various temperatures. At high field the Zeeman splitting of an oscillation peak was robust, which was gradually smeared out with raising temperature. (c) FFT spectra of the oscillations at different temperatures. The insets show the amplitudes of the FFT spectra at various temperatures. The solid lines are the fitting by the Lifshitz-Kosevich formula.

the low range of magnetic field. The fit of the temperature dependence of the FFT amplitude by the Lifshitz-Kosevich (LK) formula [43], $\Delta R_{xx}(T,B)/\Delta R_{xx}(B=0) \propto \frac{2\pi^2 k_B T m^*/eB}{\sinh(\frac{2\pi^2 k_B T m^*}{eB})}$, yields the effective cyclotron mass of two bands, respectively, $m_\beta = 0.063 m_0$ and $m_\gamma = 0.1 m_0$, where e,m_0, m^*, and k_B are, respectively, the electron charge, the free-electron mass, the effective mass of the band carriers, and the Boltzmann constant. The same results were also obtained correspondingly in other samples.

Since the dHvA effect originates directly from the oscillations of the electron's free energy, it can provide more direct information on the Fermi surface [44,45]. Figure 3(a) shows the isothermal in-plane magnetization [i.e., $B\|(012)$ surface plane] at different temperatures measured with fields up to 7 T. The magnetization data reveal pronounced dHvA oscillations. After subtracting a smooth background, the oscillatory component of ΔM versus $1/B$ is shown in Fig. 3(b). The FFT of the dHvA oscillations yields two major frequencies at $F_\alpha = 3.8$ T and $F_\gamma = 153.5$ T as shown in Fig. 3(c). The frequency of 153.5 T is close to the frequency at 162 T measured by the SdH effect, but the frequency at $F_\alpha = 3.8$ T is much lower than $F_\beta = 18$ T measured by the SdH effect. We think the different values for the lower frequencies obtained by different methods must come from the same pocket of the band. We will discuss this issue qualitatively later on in the paper. Based on the dHvA data, the cross-sectional areas of the Fermi surface normal to the field are [46] $S_\alpha = \frac{2\pi e F_\alpha}{\hbar} = 3.62 \times 10^{-4}$ Å^{-2} and $S_\gamma = \frac{2\pi e F_\gamma}{\hbar} = 1.46 \times 10^{-2}$ Å^{-2}. By assuming a circular cross section, a very small Fermi momentum $k_\alpha = \sqrt{\frac{S_\alpha}{\pi}} = 1.07 \times 10^{-2}$ Å^{-1} and $k_\gamma = \sqrt{\frac{S_\gamma}{\pi}} = 0.0682$ Å^{-1} is estimated. The dHvA oscillation can be described by the Lifshitz-Kosevich formula [47]:

$$\Delta M \propto R_T R_D \sin\left[2\pi\left(\frac{F}{B} - \gamma - \delta\right)\right],$$

where $R_T = \alpha T\mu/[B\sinh(\alpha T\mu)]$ is the thermal damping factor and $R_D = \exp(-\frac{\alpha T_D \mu}{B})$ is the Dingle damping factor. T_D is the Dingle temperature, $\mu = \frac{m^*}{m_0}$, and $\alpha = \frac{2\pi^2 k_B m_0}{\hbar e}$. The oscillation of ΔM is described by $\sin[2\pi(\frac{F}{B} - \gamma - \delta)]$ in which $\gamma = \frac{1}{2} - \phi_B/2\pi$ and ϕ_B is the Berry phase. δ is an extra phase factor that depends on the dimensionality of the Fermi surface and takes the value 0 or $\pm 1/8$ ($-$ for electronlike and $+$ for holelike) for two and three dimensions, respectively. We fitted the temperature dependence of the amplitude to the equation of $R_T = \alpha T\mu/[B\sinh(\alpha T\mu)]$ [31], yielding $m_\alpha = 0.044 m_0$ and $m_\gamma = 0.1 m_0$, as shown in Fig. 3(d). The Dingle temperature T_D for the F_γ oscillation component is found to be 10.0 K from the slope in the semilog plot of R_D at 2 K, shown in the inset of Fig. 3(d). The corresponding quantum relaxation time $\tau_q = \frac{\hbar}{4\pi^2 T_D k_B}$ is 1.214 $\times 10^{-13}$ s, from which the quantum mobility $\mu_q = e\tau/m_\gamma^\star$ is estimated to be 2134.5 cm^2/V s.

It is generally considered that the Berry phase close to π for the quantum oscillation spectra is strong evidence for topological nontrivial bands. Figure 3(e) presents the Landau-level fan diagram for the two Fermi pockets, where the maxima of the dHvA oscillations are assigned as $n + 1/4$ and the minima are assigned as $n - 1/4$ (n denotes the integer LL indices) [48]. From the linear extrapolation of the index plot, the intercepts n_{inter} are, respectively, -0.66 for $F_\alpha = 3.8$ T and 0.37 for $F_\gamma = 153.5$ T. From the values of the intercepts, the estimated Berry phase $\phi_B = 2\pi(n_{\text{inter}} + \delta)$ is -1.06π for the α band and 0.99π for the γ band, which clearly suggests that the bands in gray arsenic are nontrivial. To verify our results regarding the Berry phase, we also used the LK formula to fit the dHvA oscillation at 2 K. After filtering the lower-frequency component, the higher-frequency component at 2 K can be obtained and the oscillation of ΔM is described by the sine term with the phase factor $-\gamma - \delta$, in which $\gamma = \frac{1}{2} - \frac{\phi}{2\pi}$, shown in Fig. 3(f) [49,50]. By fitting the oscillation pattern to the LK formula (red solid line), we obtained the phase factor $-\gamma - \delta$ of -0.12, from which the Berry phase ϕ_B is determined to be 1.01π for $\delta = 1/8$, which is consistent with that of linear fitting. We also obtained the Dingle temperature of 9.8 K, and the effective mass is $0.1 m_0$. This result is also consistent with the previous one by SdH study.

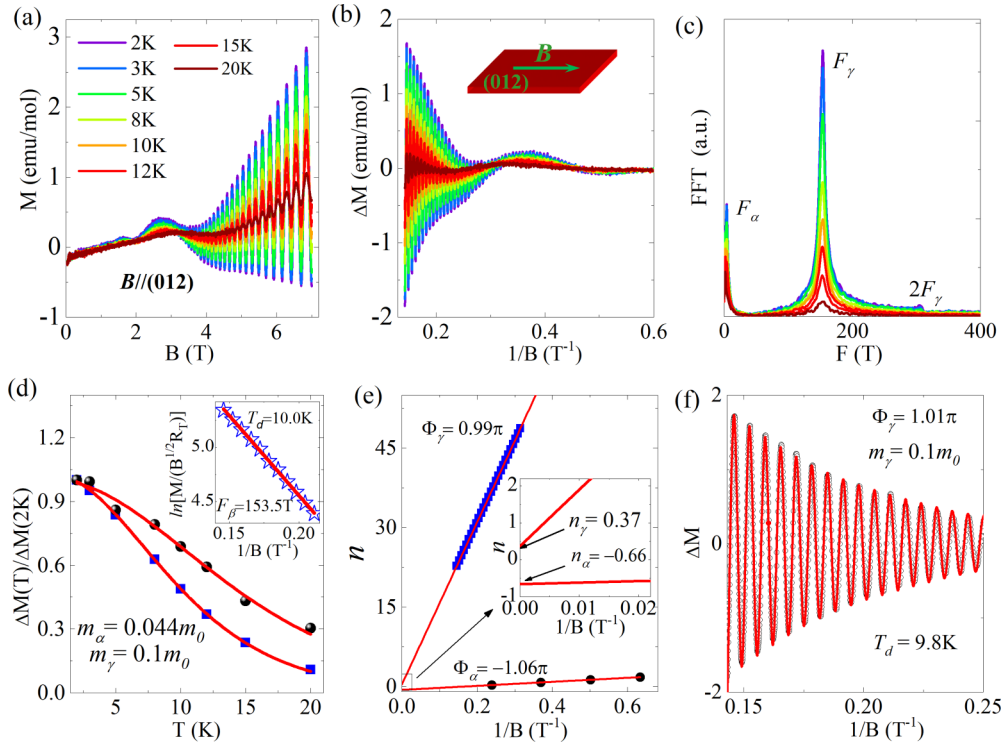

FIG. 3. (a) Isothermal in-plane magnetization at different temperatures. (b) The temperature dependence of the dHvA oscillations vs $1/B$ obtained after the subtraction of the background. (c) The corresponding FFT spectrum of the dHvA oscillations. (d) The temperature dependence of corresponding FFT amplitudes. The solid lines represent the fit for effective mass. The inset shows the Dingle plot for the high-frequency oscillation component ($F = 153.5$ T) at 2 K. (e) Landau index n plotted against $1/B$ from the dHvA oscillations. The solid lines are the linear fitting results. The inset shows the enlargement of the fittings near the origin. (f) The fitting of the high-frequency oscillation component (black data points) to the LK formula. The black circles are experimental data, and the solid line is the fitting curve.

Figure 4(a) shows the isothermal out-of-plane magnetization at different temperatures. We also observed strong dHvA oscillations, which provided us with an opportunity to further investigate the Dirac fermion properties of gray arsenic. In Fig. 4(b) we show the oscillation component ΔM by subtracting a polynomial background. The FFT of ΔM yields two major frequencies at $F_\alpha = 4.2$ T and $F_\gamma = 158.5$ T, as shown in Fig. 4(c), and the cross-sectional areas of the Fermi surface are $S_\alpha = \frac{2\pi e F_\alpha}{\hbar} = 4.0 \times 10^{-4}$ Å^{-2} and $S_\gamma = \frac{2\pi e F_\gamma}{\hbar} = 1.51 \times 10^{-2}$ Å^{-2}, respectively. By fitting the temperature dependence of the amplitude to the LK formula, the effective masses corresponding to these two frequencies are $m_\alpha = 0.048 m_0$ and $m_\gamma = 0.11 m_0$, respectively. By fitting the high-frequency oscillation at 2 K with the LK equation, we get the Berry phase at $\phi_B = 1.05\pi$ for $\delta = 1/8$, $m^* = 0.1 m_0$, and the Dingle temperature is $T_d = 8$ K.

We found that both of the main frequencies measured by the dHvA measurement are lower than the corresponding oscillation frequencies measured by the SdH measurement. In a metal, electron transport is governed by scattering mechanisms, which always varies with the number of available states into which electrons can be scattered. Resistance can be complicated by the detailed scattering mechanisms, which leads the observed SdH oscillation to deviate from the prediction by the LK theory. Whereas the dHvA oscillation originates from the oscillations of the electrons' free energy and is not affected by the scattering mechanism, it can be well fitted to the LK model. Hence, the frequency of SdH oscillations is only an approximation and is often bigger than that of dHvA oscillations in many topological semimetals, such as ZrSiS [51] and LaBi [52].

It is known that density functional theory (DFT) calculations without SOC show that the band crossings near the Fermi level form a nodal line. Considering SOC, the band crossings are fully gapped. The three-dimensional FS in the first BZ consists of three electron pockets around L and one multiply connected hole pocket around the T point. Complex Fermi surfaces can generate multiple extremal orbits that may be detectable by quantum oscillation measurements. By carefully comparing our experimental and computational results, we found when the FSs cross with the orange and purple planes perpendicular to the (012) direction in Fig. 5(a), two crossing sections are locally extremal momentum-space areas of $S_\alpha = 2.5 \times 10^{-4}$ Å^{-2} and $S_\gamma = 1.46 \times 10^{-2}$ Å^{-2}, which are roughly consistent with the observed oscillation frequencies of $F_\alpha = 4.2$ T and $F_\gamma = 158.5$ T in the dHvA effect, respectively. These two FSs of hole pockets can be seen from the band structure along the A-B and M-T paths chosen to pass through these two FSs. It is well known that when an electron circles a Dirac node in the cyclotron motion, it can accumulate a geometrical phase of π. If the Dirac node is gapped, the cycling electron will have a finite mass m proportional to the gap size, and the accumulated geometrical phase will decrease from π linearly with m [53]. As depicted in the inset of Fig. 5(b), without SOC the band along M-T is gapped to 2 meV since it deviates slightly from the nodal

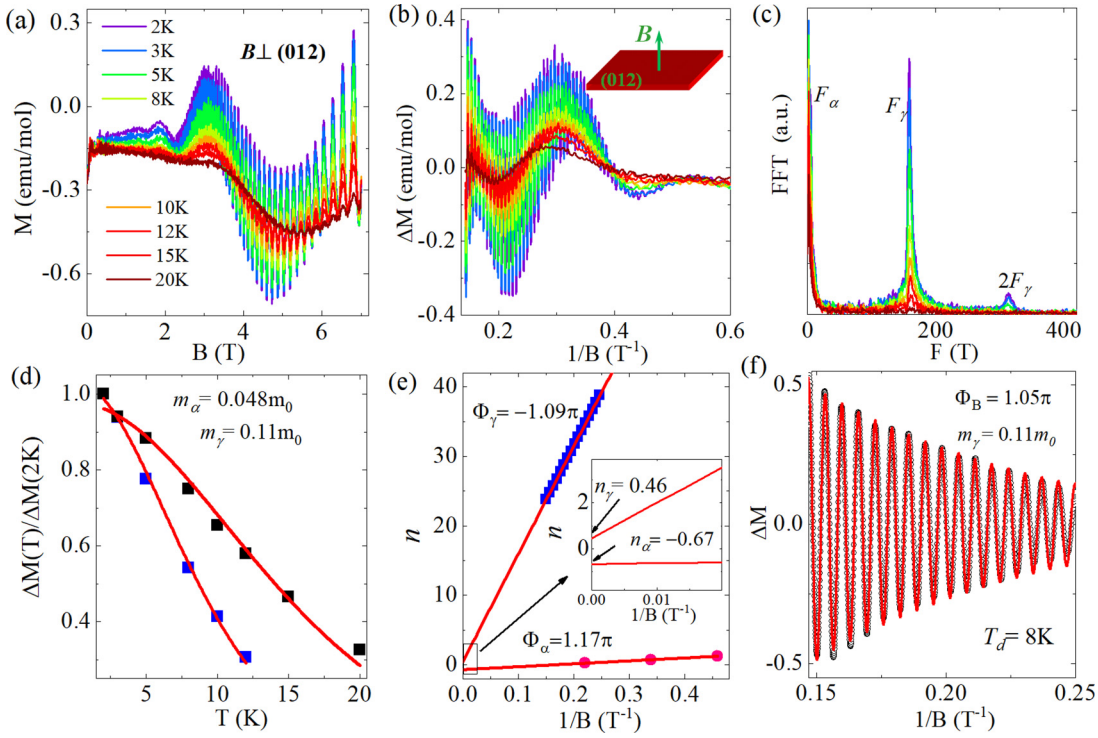

FIG. 4. (a) Isothermal out-of-plane magnetization under different temperatures. (b) The temperature dependence of the dHvA oscillations vs $1/B$ obtained after the subtraction of the background. (c) The corresponding FFT spectrum of the dHvA oscillations. (d) The temperature dependence of corresponding FFT amplitudes. The solid lines represent the fit for effective mass. (e) Landau index n plotted against $1/B$ from the dHvA oscillations. The solid lines are the linear fitting results. The inset shows the enlargement of the fitting near the origin. (f) Fitting of the high-frequency oscillation component (black data points) to the LK formula. The black circles are experimental data and the solid line is the fitting curve.

line, and SOC enhances the gap to 10 meV. If the tiny band gap is neglected, a nearly linearly dispersive crossing along M-T just above E_F enclosed by the α pocket may contribute to a Berry phase $\sim\pi$, in agreement with the analysis from the dHvA oscillations. Along the line A-B passing through the calculated S_γ, the FS crosses with S_γ origins from the band with a 50 meV (150 meV) gap near the E_F without (with) SOC. The quasilinear dispersion may play a role in giving a Berry phase of 1.17π as suggested by dHvA oscillations, although the gap is much larger than that of the α pocket.

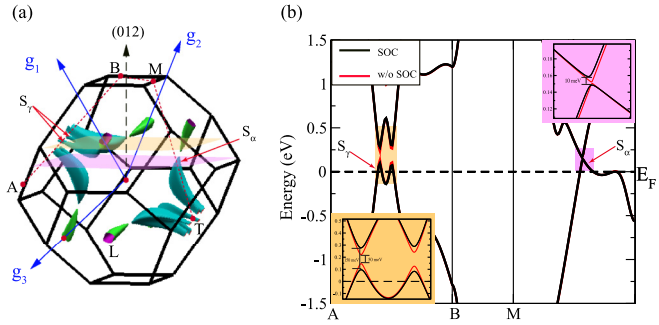

FIG. 5. (a) The FS in the first Brillouin zone (BZ). The locally extremal momentum-space areas on the orange and purple planes are pointed out by red arrows and are clearly visible. Four momenta for band-structure calculation are A (0.095, −0.083, 0.144), B (−0.071, 0.124, 0.144), M (0.000, 0.183, 0.048), T (0.000, 0.000, −0.144) in units of $2\pi/a$. (b) Band structure along A-B-M-T with (black) and without (red) spin-orbital coupling (SOC).

To investigate the detailed angular dependence of the magnetization, we performed dHvA effect experiments with the magnetic field being rotated from the out-of-plane to the in-plane direction, as shown in Fig. 6(a), where the magnetic field normal to the (012) plane is defined as zero degrees, $\theta = 0^\circ$. After subtracting a smooth background, we obtained the dHvA oscillations versus $1/B$ curves at various angles, as shown in Fig. 6(b). It is interesting that the amplitude of the oscillations decreases with the increase of the angle and becomes almost undetectable at an angle of 30°. Beyond 30°, the oscillations appear again, and the amplitude increases with the increase of the angles. This feature can be understood as follows: Since the (012) plane is not the high-symmetry surface, it has an angle of 60° with the (001) plane [see the inset of Fig. 6(d)]. When the magnetic field is applied with $\theta = 30^\circ$, it corresponds to the case with a magnetic field exactly along the (001) plane of the crystal, i.e., the $B||ab$ plane, at which the amplitude of the quantum oscillation is the smallest based on the band calculation [24].

To figure out the angular-dependent Fermi surface topology, we perform the FFT on the dHvA oscillations at each angle and get the dominant oscillation frequencies, respectively, which are depicted in Fig. 6(c). Figure 6(d) presents the angular-dependence oscillatory frequencies. The low-frequency F_α branch almost remains unchanged with the angles $\theta > 20^\circ$, and then slightly increases, indicating the

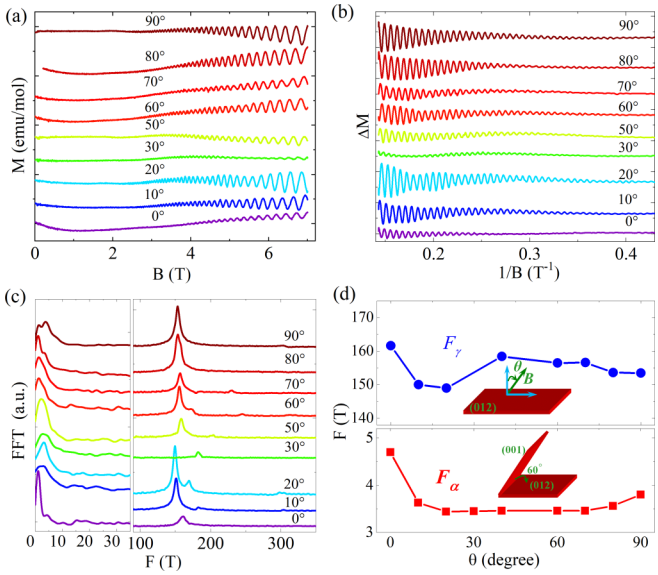

FIG. 6. (a) The magnetization was measured under different tilted angles and had been shifted for clarity. (b) The oscillatory component ΔM, extracted from M by subtracting a smooth background, as a function of $1/B$ under different magnetic field orientations. (c) FFT spectra of the dHvA oscillations. (d) Angular dependence of the quantum oscillation frequency of α band and γ band, respectively.

quasi-isotropic feature. In contrast, the F_γ branch shows a very weak angular dependence in the whole angle range. The observed angular dependence of oscillation frequencies of gray arsenic implies that gray arsenic possesses 3D-like Fermi surfaces, and both bands show a clearly nontrivial Berry phase. We noted that the recent ARPES and band-structure calculation by Zhang *et al.* [31] presented topologically entangled Rashba-split Shockley states on the (111) surface of gray arsenic; such 2D-like surface states are not identified by our angular dependent dHvA measurements. Our data intuitively support a Dirac semimetal character for gray arsenic, not a topological insulator. Of course, we are also aware that there has been some debate recently arguing that the nontrivial Berry phase obtained from the Landau fan of the SdH quantum oscillations may not be a reliable criterion for a topological matter. However, our results at least provide an alternative understanding of the nature of band topology of gray arsenic, which may attract more attention in both experimental and theoretical studies in the future.

IV. CONCLUSIONS

In summary, we performed systematic magnetotransport measurement under high magnetic fields on gray arsenic single crystals. We found that the bulks exhibit strong angle-dependent magnetoresistance without saturation at 40 T. We also measured the de Haas–van Alphen (dHvA) effect under an in-plane or out-of-plane magnetic field at different temperatures. Analyzing the dHvA oscillations demonstrated that this material harbors nearly massless relativistic fermions along with a nontrivial Berry phase, which provides possible evidence for the existence of a Dirac semimetal phase in gray arsenic.

ACKNOWLEDGMENTS

We thank Xiaosong Wu, Zengwei Zhu, Peifeng Fan, Huidong Li, and Yiding Liu for fruitful discussions. This work was supported by the National Key Research and Development Program of China, Grant No. 2016 YFA0401003, the Natural Science Foundation of China (Grants No. U19A2093, No. 11774353, No. 11574320, No. 11374302, No. 11674369, No. U1432251, and No. U1732274), and Collaborative Innovation Program of Hefei Science Center, CAS (Grant No. 2019HSC-CIP 001), the Innovative Program of Development Foundation of Hefei Center for Physical Science and Technology (Grant No. 2018CXFX002).

L. A. and X. Z. contributed equally to this work.

[1] Politano, G. Chiarello, Z. L. Li, V. Fabio, L. Wang, L. W. Guo, X. L. Chen, and D. W. Boukhvalov, Adv. Funct. Mater. **28**, 1800511 (2018).

[2] C. R. Rajamathi, U. Gupta, N. Kumar, H. Yang, Y. Sun, V. Süß, C. Shekhar, M. Schmidt, H. Blumtritt, and P. Werner *et al.*, Adv. Mater. **29**, 1606202 (2017).

[3] M. H. Engelkamp, F. Apuzzo, A. D. Gaspare, P. D. Pietro, I. Lo Vecchio, M. Brahlek, N. Koirala, S. Oh, and S. Lupi, ACS Photon. **2**, 1231 (2015).

[4] P. D. Pietro, M. Ortolani, O. Limaj, A. D. Gaspare, V. Giliberti, F. Giorgianni, M. Brahlek, N. Bansal, N. Koirala, and S. Oh *et al.*, Nat. Nanotechnol. **8**, 556 (2013).

[5] A. Politano, C. Lamuta, and G. Chiarello, Appl. Phys. Lett. **110**, 211601 (2017).

[6] A. Politano, V. M. Silkin, I. A. Nechaev, M. S. Vitiello, L. Viti, Z. S. Aliev, M. B. Babanly, G. Chiarello, P. M. Echenique, and E. V. Chulkov, Phys. Rev. Lett. **115**, 216802 (2015).

[7] J. D. Yao, Z. Q. Zheng, and G. W. Yang, Adv. Funct. Mater. **27**, 1701823 (2017).

[8] A. Politano, L. Viti, and M. S. Vitiello, APL Mater. **5**, 035504 (2017).

[9] W. W. Tang, A. Politano, C. Guo, W. L. Guo, C. L. Liu, L. Wang, X. S. Chen, and W. Lu, Adv. Funct. Mater. **28**, 1801786 (2018).

[10] L. Viti, D. Coquillat, A. Politano, K. A. Kokh, Z. S. Aliev, M. B. Babanly, O. E. Tereshchenko, W. Knap, E. V. Chulkov, and M. S. Vitiello, Nano Lett. **16**, 80 (2016).

[11] F. Tang, H. C. Po, A. Vishwanath, and X. G. Wan, Nature (London) **566**, 486 (2019).

[12] T. T. Zhang, Y. Jiang, Z. D. Song, H. Huang, Y. Q. He, Z. Fang, H. M. Weng, and C. Fang, Nature (London) **566**, 475 (2019).

[13] M. G. Vergniory, L. Elcoro, C. Felser, N. Regnault, B. A. Bernevig, and Z. J. Wang, Nature (London) **566**, 480 (2019).

[14] B. A. Bernevig, T. L. Hughes, and S. C. Zhang, Science **314**, 1757 (2006).

[15] L. Fu and C. L. Kane, Phys. Rev. B **76**, 045302 (2007).
[16] J. Wang, A. Alexandradinata, R. J. Cava, and B. A. Bernevig, Nature (London) **532**, 189 (2016).
[17] B. J. Wieder, B. Bradlyn, Z. J. Wang, J. Cano, Y. Ki, H. D. Kim, A. M. Rappe, C. L. Kane, and B. A. Bernevig, Science **361**, 246 (2018).
[18] Z. Wang, H. M. Weng, Q. S. Wu, X. Dai, and Z. Fang, Phys. Rev. B **88**, 125427 (2013).
[19] Z. J. Wang, Y. Sun, X. Q Chen, C. Franchini, G. Xu, H. M. Weng, X. Dai, and Z. Fang, Phys. Rev. B **85**, 195320 (2012).
[20] H. Weng, C. Fang, Z. Fang, B. A. Bernevig, and X. Dai, Phys. Rev. X **5**, 011029 (2015).
[21] S. M. Huang, S. Y. Xu, I. Belopolski, C. C. Lee, G. Q. Chang, B. K Wang, N. Alidoust, G. Bian, M. Neupane, and C. L. Zhang *et al.*, Nat. Commun. **6**, 7373 (2015).
[22] S.-Y. Xu, I. Belopolski, N. Alidoust, M. Neupane, G. Bian, C. L. Zhang, R. Sankar, G. Q. Chang, Z. J. Yuan, and C. C. Lee *et al.*, Science **349**, 613 (2015).
[23] T. Bzdusek, Q. S. Wu, A. Ruegg, M. Sigrist, and A. A. Soluyanov, Nature (London) **538**, 75 (2016).
[24] B. Bradlyn, J. Cano, Z. J. Wang, M. G. Vergniory, C. Felser, R. J. Cava, and B. A. Bernevig, Science **353**, aaf5037 (2016).
[25] Z. K. Liu, B. Zhou, Y. Zhang, Z. J. Wang, H. M. Weng, D. Prabhakaran, S.-K. Mo, Z. X. Shen, Z. Fang, and X. Dai *et al.*, Science **343**, 864 (2014).
[26] D. T. Son and B. Z. Spivak, Phys. Rev. B **88**, 104412 (2013).
[27] H. B. Nielsen and M. Ninomiya, Phys. Lett. B **130**, 389 (1983).
[28] V. Aji and A. B. Jackiw, Phys. Rev. B **85**, 241101 (2012).
[29] J. Hu, Z. J. Tang, J. Y. Liu, Y. L. Zhu, J. Wei, and Z. Q. Mao, Phys. Rev. B **96**, 045127 (2017).
[30] J. H. Xu, E. G. Wang, C. S. Ting, and W. P. Su, Phys. Rev. B **48**, 17271 (1993).
[31] P. Zhang, J. Z. Ma, Y. Ishida, L. X. Zhao, Q. N. Xu, B. Q. Lv, K. Yaji, G. F. Chen, H. M. Weng, and X. Dai *et al.*, Phys. Rev. Lett. **118**, 046802 (2017).
[32] L. X. Zhao, Q. N. Xu, X. M. Wang, J. B. He, J. Li, H. X. Yang, Y. J. Long, D. Chen, H. Liang, and C. H. Li *et al.*, Phys. Rev. B **95**, 115119 (2017).
[33] G. Kresse and J. Furthmüller, Phys. Rev B **54**, 11169 (1996).
[34] P. E. Blöchl, Phys. Rev B **50**, 17953 (1994).
[35] G. Kresse and D. Joubert, Phys. Rev B **59**, 1758 (1999).
[36] J. P. Perdew, K. Burke, and M. Ernzerhof, Phys. Rev. Lett. **77**, 3865 (1996).
[37] A. A. Mostofi, J. R. Yates, G. Pizzi, Y.-S. Lee, I. Souza, D. Vanderbilt, and N. Marzari, Comput. Phys. Commun. **185**, 2309 (2014).
[38] Q. S. Wu, S. N. Zhang, H. F. Song, M. Troyer, and A. A. Soluyanov, Comput. Phys. Commun. **224**, 405 (2018).
[39] C. L. Zhang, C. Guo, H. Lu, X. Zhang, Z. J. Yuan, Z. Q. Lin, J. F. Wang, and S. Jia, Phys. Rev. B **92**, 041203(R) (2015).
[40] M. N. Ali, J. Xiong, S. Flynn, J. Tao, Q. D. Gibson, L. M. Schoop, T. Liang, N. Haldolaarachchige, M. Hirschberger, and N. P. Ong *et al.*, Nature (London) **514**, 205 (2014).
[41] C. Shekhar, A. K. Nayak, Y. Sun, M. Schmidt, M. Nicklas, I. Leermakers, U. Zeitler, Y. Skourski, J. Wosnitza, and Z. K. Liu *et al.*, Nat. Phys. **11**, 645 (2015).
[42] X. C. Huang, L. X. Zhao, Y. J. Long, P. P. Wang, D. Chen, Z. H. Yang, H. Liang, M. Q. Xue, H. M. Weng, and Z. Fang *et al.*, Phys. Rev. X **5**, 031023 (2015).
[43] H. Murakawa, M. S. Bahramy, M. Tokunaga, Y. Kohama, C. Bell, Y. Kaneko, N. Nagaosa, H. Y. Hwang, and Y. Tokura, Science **342**, 1490 (2013).
[44] M. V. Kartsovnik, Chem. Rev. **104**, 5737 (2004).
[45] I. M. Lifshitz and A. M. Kosevich, Sov. Phys. JETP **2**, 636 (1956).
[46] D. Shoenberg, *Magnetic Oscillations in Metals* (Cambridge University Press, Cambridge, England, 1984).
[47] G. P. Mikitik and Y. V. Sharlai, Phys. Rev. Lett. **82**, 2147 (1999).
[48] Y. Ando, J. Phys. Soc. Jpn. **82**, 102001 (2013).
[49] Y. B. Zhang, Y. W. Tan, H. L. Stormer, and P. Kim, Nature (London) **438**, 201 (2005).
[50] G. P. Mikitik and Y. V. Sharlai, Phys. Rev. Lett. **93**, 106403 (2004).
[51] M. Matusiak, J. R. Cooper, and D. Kaczorowski, Nat. Commun. **8**, 15219 (2017).
[52] R. Singha, B. Satpati, and P. Mandal, Sci. Rep. **7**, 6321 (2017).
[53] B. B. Andrei and T. L. Hughes, *Topological Insulators and Topological Superconductors* (Princeton University Press, Princeton, NJ, 2013).

Correction: The affiliation indicators for the sixth and seventh authors contained errors and have been fixed.